CIENTIFIC Publishing Limited

Prevention and Treatment of Natural Disasters

http://ojs.ukscip.com/index.php/ptnd

Article

Designing Post-Fire Flood Protection Techniques for a Real Event in Central Greece

Angelos Alamanos [1], George Papaioannou [2,*], George Varlas [3], Vassiliki Markogianni [3], Angelos Plataniotis [4,5], Anastasios Papadopoulos [3], Elias Dimitriou [3] and Phoebe Koundouri [4,6,7]

[1] Independent Researcher, 10243 Berlin, Germany
[2] Department of Forestry and Management of the Environment and Natural Resources, Democritus University of Thrace, 68200 Orestiada, Greece
[3] Hellenic Centre for Marine Research, Institute of Marine Biological Resources and Inland Waters, 19013 Anavissos, Greece
[4] Sustainable Development Unit, Athena Research Center (RC), 15125 Athens, Greece
[5] Department of Economics, National and Kapodistrian University of Athens, 10559 Athens, Greece
[6] School of Economics and Research Laboratory on Socio-Economic and Environmental Sustainability, Athens University of Economics and Business, 10434 Athens, Greece
[7] Department of Technology, Management and Economics, Denmark Technical University (DTU), 2800 Kongens Lyngby, Denmark
[*] Correspondence: gpapaio@fmenr.duth.gr

Received: 25 June 2024; **Revised**: 12 July 2024; **Accepted**: 23 July 2024; **Published**: 4 September 2024

Abstract: Wildfires pose a growing global danger for ecosystems and human activities. The degraded ecosystem functions of burnt sites, include, among others, shifts in hydrological processes, land cover, vegetation, and soil erosion, that make them more vulnerable to flood and extreme sediment transport risks. Several post-fire erosion and flood protection treatments (PFPs) have been developed to avoid and mitigate such consequences and risks. The Mediterranean region faces severe climate change challenges that are projected to escalate the wildfire and post-fire flood risks. However, there is limited research on the dynamics of post-fire flood risks and their mitigation through the design of the appropriate PFPs. This paper aims to cover this gap by simulating a real post-fire flash-flood event in Central Greece, and design the PFPs for this case study, considering their suitability and costs. An integrated framework was used to represent the flood under the baseline scenario: the storm conditions that caused the flood were simulated using the atmospheric model WRF-ARW; the burn extent, severity, and the flood extent were retrieved through remote sensing analyses; and a HEC-RAS hydraulic-hydrodynamic model was developed to simulate the flood event, applying the rain-on-grid technique. Several PFPs were assessed, and certain channel- and barrier-based PFPs were selected as the most suitable for the study area. The recommended PFPs were spatially represented within a geographic information system (GIS). Moreover, we present a detailed analysis of their expected costs. This study provides an interdisciplinary and transferable framework for understanding and enhancing the flood resilience of burnt sites.

Keywords: post-fire; flash-floods; post-fire protection; hydraulic modeling; remote sensing; costs; techno-economic analysis

1. Introduction

The increasing prevalence and severity of wildfires, exacerbated by a changing climate globally, pose a pressing challenge with far-reaching consequences for ecosystems and human communities [1–3]. Mediterranean countries have been characterized as climate hot-spots [4], being particularly vulnerable to wildfires of increased severity each coming summer [5–7]. Wildfires significantly change the land cover, vegetation, soil conditions, hydromorphology, and the hydrological-hydraulic behavior of affected catchments under intense storm events [8]. This causes altered runoff patterns, reduced infiltration, increased streamflow rates and sediment transport for burnt sites, making them more susceptible to extreme peak-flows and flood hazards [9–11]. Understanding and mitigating these hazards is crucial, given the rising global threats from compound events, such as wildfires and extreme storms [12,13], and Mediterranean countries are among the priority areas for timely resilience-building [14,15]. In order to speed up the restoration and recovery of the hydrological processes of burnt sites, several practices have been developed, known as post-fire erosion and flood protection treatments (PFPs). These can be cover-based and include barriers, mulch or hydromulch, erosion control mats, silt fences, seeding, or in-channel treatments, such as check dams, grade stabilizers, in-channel tree felling, debris basins, stream channel armoring, while road and trail or even chemical treatments can be used [16].

The response of a burnt catchment to an extreme storm largely depends on multiple factors (fire- and non-fire-related) that interact, so their thorough modeling is crucial for understanding the post-fire flood dynamics, and ultimately designing the appropriate protection measures. However, model-based assessments of such fire- and non-fire-related factors are scarce in the literature, mainly due to their computational complexity [17]. Also, the design of the most suitable PFPs is a challenging, and quite overlooked topic, as it can be very case-specific, and there is limited literature to provide general guidelines [18,19]. In this paper we aim to fill these gaps by: i) simulating a real post-fire flash-flood event that occurred in a typical Mediterranean catchment (Kineta, Greece); ii) assessing and recommending the most suitable PFPs, designing them spatially and estimating their costs.

The simulation of the flood event included the modeling of the main factors (as mentioned, fire- and non-fire-related factors) that affect the flooding. First, understanding the storm conditions that caused the flood (physical and meteorological characteristics) is a key factor [20,21]. For the storm simulation, the Advanced Weather and Research Forecasting (WRF-ARW) v4.2 model was used [22]. The WRF-ARW atmospheric model has been successfully used in previous applications for the simulation of meteorological phenomena in several case studies, and Greek ones. These applications include heavy precipitation events and storms, and their forecast [23–26]. Second, the burn severity and extent directly affect the hydrological response. These were assessed by remote sensing (RS) techniques. RS is very common in studies relevant both to wildfires and floods, and in general, particularly useful for obtaining ready-to-use information that is not available through on-site observations [19,27,28]. In particular, RS has been used to assess wildfire impacts such as burn severity [29], burn extent and site recovery [30], along with various other applications [31]. Also, the flood extent was identified by RS. RS applications have been widely used for identifying flooded areas [32] with satisfactory performance and spatial detail [33,34]. Third, a hydraulic model was developed to simulate how the storm precipitation estimated by the WRF-ARW formed the flood extent (as obtained by the RS application). The 2D Hydrologic Engineering Center's River Analysis System (HEC-RAS, version 6.4.1) was used for this task, as it is a common software for flood inundation mapping [35] which has been successfully performed under various scales [25,36,37] and data availability conditions [38,39]. Although there are studies using similar approaches, the combination of these tools to simulate a real flood event is a novel application. Previous studies have explored the flood response of burnt sites primarily from the lens of hydrological modeling, underscoring the need for the timely application of PFPs, given the increased post-fire flood risks [40]. The growing recognition of the need for PFPs to mitigate flood risks has encouraged more studies exploring the role of PFPs, mostly experimental though [41–43]. However, the literature on the PFP design and costs is still poor, and underrepresented in countries outside the US, Spain and Portugal [41,42]. In their review article on PFPs, Lopes et al. [44] found that only 27% of the papers assessed have performed model-based assessments on the role of PFPs. Indeed, the few studies exploring the role of PFPs, usually do not reflect on their design principles (namely, how and why to choose the most suitable PFPs), and focus on soil erosion and sediment transport mitigation, not flooding [45–49]. So, the fourth element of this study aims to contribute to this issue by using the insights of the

flood simulation model, the available literature, guidelines and general practice, to design the most suitable PFPs for the study area, representing them spatially. Another crucial factor for flood-protection-related decisions is the investments needed, but the literature still lacks thorough PFP-cost analyses [50–52], with the exception of a handful of national guidelines available [53]. Therefore, we performed a PFP-cost analysis, providing a detailed and transferable break-down of the cost components.

This paper not only provides valuable insights for a better understanding of the post-fire flood responses, but also facilitates the design of PFPs and their economic implications, ultimately offering transferable knowledge to other study areas to address the future risks from wildfires and their associated flood consequences.

2. The Post-Fire Flood in Kineta Catchment, Greece

The case study application area is the Kineta catchment in western Attica, central Greece—a Mediterranean area covering approximately 40 km^2. The northern part of Kineta drains water flows from the Geraneia mountains to its outlet to the sea in the southern part, around the coastal town of Kineta, through one main stream and a few smaller ones (Figure 1). The climate follows the typical Mediterranean pattern, characterized by hot and dry summers, and mild and rainy winters (Table 1).

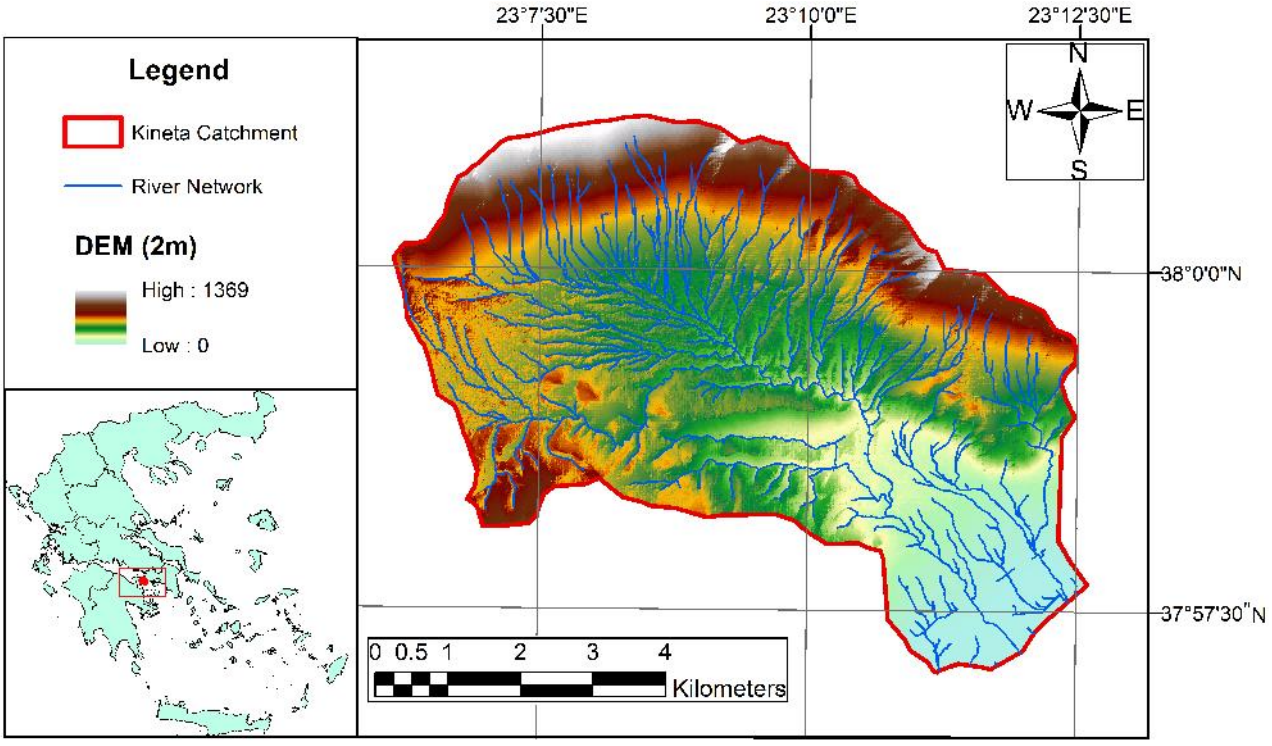

Figure 1. The Kineta catchment in Greece.

Table 1. Average monthly values of precipitation and temperature in Kineta (Data: 1991–2021, Source: reference [54]).

Month	Average Precipitation (mm)	Average Temperature (°C)
January	58	8.3
February	52	8.9
March	53	11.3
April	25	14.7
May	20	19.5
June	7	24.2
July	4	26.8
August	3	26.7
September	18	22.8
October	33	18.3
November	56	13.9
December	65	9.9

The area has a history of wildfire threats, with notable incidents in the summers of 2017 and especially 2018. The 2018 fire consumed the pine forest of Geraneia mountains, and burned down the nearby settlements (Panorama and Galini), as well as houses in the town of Kineta, causing many injuries (Figure 2).

Figure 2. Indicative photos of the damages in the Kineta catchment by the wildfire of 2018, spanning from the mountainous pine forest to the coast [55–58].

A visual inspection after the 2018 wildfires, reported that there were some PFPs in place, mainly aiming to protect the road network from landslides [55]. In particular, only a few log-erosion barriers (LEBs) were placed alongside the Geraneia road bridge, parallel to the contours, but as reported, they were not properly installed [55]. The following year, 2019, an extreme storm caused a destructive flash-flood (November 24–26). The flood brought downstream a considerable amount of sediment mainly through the streams (mud, trees, rocks, etc.), which, combined with the large volume of water, caused severe damages (Figure 3). It is also reported that even before the storm, the areas' streams were blocked by sediments that have been accumulated since the wildfire [55]. The wildfire probably contributed to some extent to this flood event, as the area had not adequately recovered in terms of forest, land cover and vegetation conditions, and there were blocked streams by sediments. Also, the PFPs were proved to be insufficient as they were probably not well-installed and maintained, and were not particularly targeted for flood protection.

Figure 3. Damages by the flood of 2019 to infrastructure, road networks, and the coastline of the Kineta area [55–57].

3. Methodology

3.1. Hydro-Meteorologic Model

The simulation of the storm of November 2019 by the WRF-ARW model was implemented with three nested domains with horizontal grid spacings of 9 km, 3 km, and 1 km, covering a wide area from Europe to West Asia, Greece, and the flooded area, respectively. The storm that caused the flash flood in Kineta took place on 24–25 November 2019. So, the simulation was configured for 48 hours from November 24 at 00:00 UTC (02:00 local time) up to November 26 at 00:00 UTC (02:00 local time). Global Forecasting System (GFS) data on a horizontal grid spacing of 0.25° × 0.25° were used for the definition of the initial and boundary conditions. The initial conditions involved atmospheric forcing data at several atmospheric pressure levels and near the surface, as well as soil moisture and temperature. The sea surface temperature (SST) in the lower boundary conditions of the simulation was updated every 6 hours and they were constructed using real-time global (RTG) SST analysis data,

on a horizontal grid spacing of 0.083° × 0.083° [59]. The parameterization of the ground processes was achieved through the unified Noah land surface model [26]. The RRTMG scheme was employed for the parameterization of the long-wave and short-wave radiation processes [60]. The cloud microphysics processes were parameterized by the WSM 5-class scheme [61]. Convective processes were handled by the Grell-Freitas ensemble scheme for the first domain (9 × 9 km) and explicit convection resolution for the other two domains (3 × 3 km and 1 × 1 km) [62]. The Yonsei University scheme (YSU) and the revised Monin-Obukhov scheme were used for the planetary boundary layer and surface layer processes [23,24,63].

3.2. Remote Sensing Application for Wildfire Effects

Three Sentinel-2 satellite images captured the Kineta catchment's burnt (1 image) and post-fire (2 images) conditions, to assess the fire's damage. These images were obtained from the Copernicus Open Access Hub [64] and were selected based on the ESA tiling grid with unique IDs for each tile (100 × 100 km ortho-images). The images were pre-processed in Q-GIS 3.6.3 using the semi-automatic classification plugin, involving their conversion from digital numbers (DN) to top-of-atmosphere (TOA) reflectance, and atmospheric correction via the widely-used DOS1 method [65]. The study area was then delineated to map the burnt areas for two periods: July to August 2018 and July 2018 to October 2019, focusing on the detection of the regrown vegetation. Burnt areas were mapped using the Normalized Burn Ratio (NBR) (Equation (1)) for both periods, with bands B08 (NIR) and B12 (SWIR) [66,67]. NBR values range from -1 to $+1$, indicating high and low values for healthy green and burnt vegetation, respectively.

$$NBR = \frac{(NIR - SWIR)}{(NIR + SWIR)} \quad (1)$$

The change in Normalized Burn Ratio (delta *NBR*—*dNBR*) was computed in two steps to highlight changes from the reference state. This involved subtracting post-fire *NBR* values (2 August 2018 and 16 October 2019) from the reference NBR value of 20 July 2018 (Equation (2)). This approach offers an accurate assessment of burn severity, as it relies on per-pixel changes in reflectance values. In accordance with Rahman et al. [31,68], a threshold value of $+0.1$ was applied to both dNBR files for each period, facilitating the appropriate differentiation of burnt and unburnt areas within the study region. The resulting dNBR values were multiplied by 1000 and classified based on burn severity ranges recommended by the United States Geological Survey (USGS). The twofold calculation of dNBR initially identified the most wildfire-affected areas for each period and subsequently illustrated changes in burn severity levels from August 2018 to October 2019.

$$dNBR = NBR_{prefire} - NBR_{postfire} \quad (2)$$

3.3. Remote Sensing Application for Flood Effects

A single Sentinel-2 image from 25 November 2019 (processing level 1C, time 09:23:21:024Z) mapped the flood-inundated areas in Kineta, aligning with the event starting on 24 November 2019. This image underwent the same pre-processing as the burnt area mapping. For water delineation, spectral indices (NDWI, MNDWI, AWEI, RSWIR1, RSWIR2) were evaluated using S2 bands. Additionally, SWIR2, *NIR*, and red bands were transformed to HSV (Hue, Saturation, Value) colors following Pekel et al.'s method [69]. Water indices were computed, each with a manually adjusted threshold for accurate delineation. Binarization produced the final 'water' images. Five water indices (WIs) were computed on the S2 image from 25 November 2019, to determine the most representative threshold value for each WI. Histogram analysis revealed distinct peak magnitudes, where positive values typically corresponded to water and negative or zero values to soil or terrestrial vegetation. Manual adjustment of thresholds was employed to enhance the accuracy of water delineation, always in relation to the actual images and drone videos of the visual inspection after the flood [55,70]. Subsequently, each image file representing a distinct WI was binarized, assigning a logical value (true) for values exceeding the threshold and false for lower values, resulting in the final 'water' images. These flooded areas served as the validation area for the hydraulic model.

3.4. Hydrodynamic Model

At this stage, the hydraulic model was set up in HEC-RAS, with the following input data:

a) The 2 m-resolution Digital Elevation Model (DEM) retrieved by the Greek National Cadastre and Mapping Agency [71];
b) the stream channel characteristics (river flowpaths and banks);
c) the storm precipitation (spatially distributed, as simulated by the WRF-ARW atmospheric model mentioned above), which was applied as a rain-on-grid input representing accurately the real storm event (time-step: 1 h, so 20 spatial datasets/grids from 24 November 2019 14:00:00 to 25 November 2019 09:00:00). This is achieved by the rain-on-grid technique, which applies the spatially distributed rainfall directly, eliminating thus the need for a pre-defined hydrograph as the primary input for surface runoff. The precipitation characteristics of the storm as estimated by the WRF-ARW model were imported into the HEC-RAS through the rain-on-grid routine on an hourly basis (as distinct spatial datasets representing different times of the storm) from 24 November 14:00:00 to 25 November 09:00:00;
d) land cover maps (pre-fire and post-fire conditions);
e) the spatially distributed Manning's roughness. In particular, the Manning's n coefficients were estimated based on typical values from the literature for similar areas in similar conditions (combined land cover types and burn severity classes), considering the fire effects [59,72–74]. In particular, the n values were considered according to the combination of the areas' land cover types (as in the CORINE2018 categorization) and the different burn severity conditions (as characterized from the RS results). Thus, for each combination of land cover type (e.g., 'complex cultivation patterns', 'coniferous forest', 'mixed forest', 'grasslands', 'road networks', etc.) with all the burn severity classes (e.g., 'enhanced regrowth high', 'enhanced regrowth low', 'high severity', 'low severity', 'moderate-low severity', 'moderate-high severity', and 'unburnt'), a roughness n value was assigned, based on typical values from references [59,72–74]. Several model-runs allowed us to calibrate the model based on the flood extent retrieved from the RS results.

The HEC-RAS simulation output was the mapping of the inundated areas with the water depth and water velocity during each time step of the studied event. The results were validated based on the flooded area polygon (obtained from the RS analysis, as mentioned above). The Critical Success Index (CSI) was used to quantify the accuracy of the simulated inundated areas against the validation area, as in Equation (3) [75,76]. A represents the correctly simulated flooded area; B is the false-simulated flooded area (false alarms); C is the flooded area that is not predicted by the model (misses).

$$CSI = \frac{A}{A + B + C} \tag{3}$$

3.5. PFP Assessment

The next step, after the hydraulic simulation of the flood event, is the PFP analysis. This included initially a brief review of the available information on each PFP type, considering their site suitability, potential effectiveness, and costs. Although there is limited available information on this topic, at least in a coherent way [16,77], the main categorization of the most commonly applied PFPs refers to [16,78]:

- Land treatments: These methods stabilize burned areas by providing soil cover, which reduces erosion, and mitigates water repellency to improve infiltration. Land treatments focus on accelerating recovery while preserving ecosystem integrity and functionality. There are two main types: cover-based (improving land cover through practices like seeding) and barrier-based (installing barriers to trap sediments, reduce excess flow, and slow runoff).
- Channel treatments: These are applied in the streams to address the adverse post-fire effects on water quality, water control, water velocity, sediment trapping, and channel characteristics, protecting critical downstream areas.
- Road and trail treatments: These are often used in conjunction with land and channel treatments, and aim to minimize the impact of fires on transportation infrastructure.

The selection of the specific PFPs from each category or their combination, was done in combination with the results of the RS and flood inundation models, and considering the available technical guidelines and each

PFP's characteristics. The selected PFPs were spatially modeled in a geographic information system (GIS). Finally, the potential costs for the application of the designed PFPs were estimated by a simple accounting process.

4. Results and Discussion

The RS analysis revealed the burn severity and extent, and their changes from the fire (August 2018) until the flood event (November 2019). The dNBR analysis indicated vegetation regrowth from August 2018 to October 2019, just before the flood: The extent of high burn severity areas was 12.5% in August 2018, and decreased to 0.01% by October 2019, transitioning primarily to 'moderate-low' burn severity areas (Figure 4A,B). Moreover, after the fire (August 2018), the unburnt areas were covering 19% of the burn extent area, while the areas with low burn severity 15.9%, and the areas with low-moderate burn severity 21%. In October 2019, the respective percentages were 24.1%, 29.3%, and 35.5%. The predominant burn severity classes in 2018 were 'moderate-high' and 'moderate-low' severity, and 'unburnt' areas, but in October 2019, the main burn severity classes were 'moderate-low', 'low' severity and 'unburnt' areas.

In this context, the storm of November 2019 occurred in the Kineta catchment. The results of the atmospheric model WRF indicated that the storm that caused the flood of November 2019 in Kineta was extreme. A deep barometric low from the west brought substantial precipitation across various regions in Greece. This low-pressure system, combined with a cold front, resulted in heavy precipitation at the broader Kineta area on the night of November 24 to 25. The meteorological station of the National Observatory of Athens (NOA) network at Agioi Theodoroi, about 8 km southwest of Kineta, recorded 206.8 mm of total rainfall during November 24 and 25 [79]. The WRF-ARW simulation estimated 182.6 mm of precipitation in the same area, closely matching the actual records (Figure 4C). Most of the precipitation occurred between November 24, 22:00 local time (20:00 UTC), and November 25, local time 08:00 (06:00 UTC), with a severe storm cell centered around Kineta during the early hours of November 25, (approximately from 03:00 to 06:00 local time). These rainfall rates were responsible for the extremely high runoff within the catchment, causing the flash-flood.

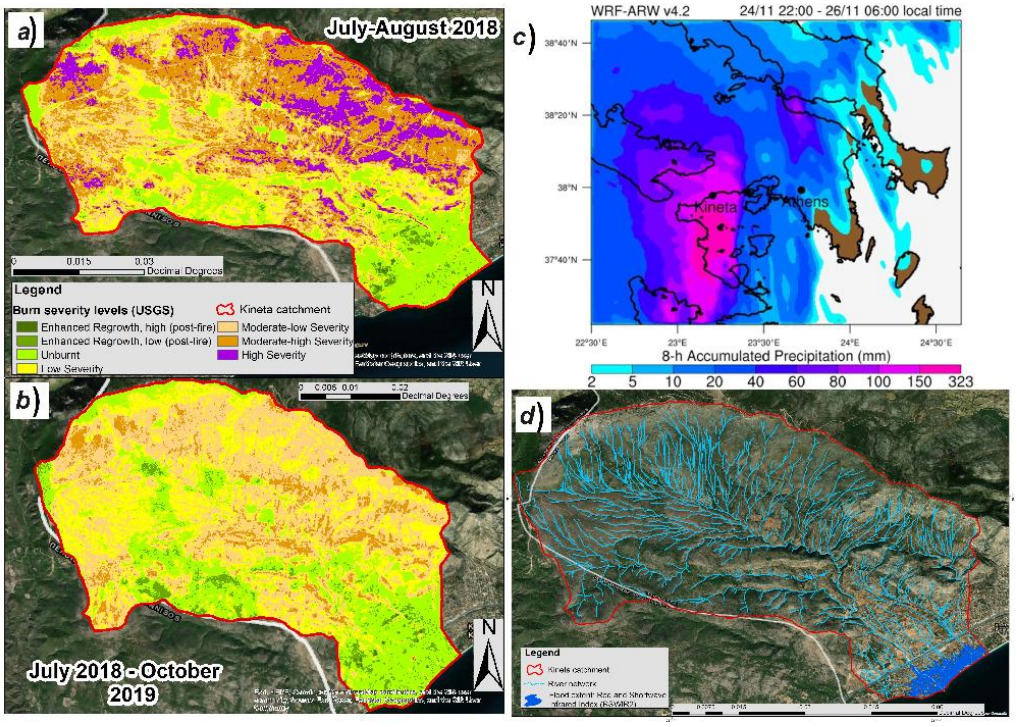

Figure 4. The RS results of the burn extent and severity were obtained. (**a**) during the wildfire period (July–August 2018); (**b**) after the fire (July 2018–October 2019), before the flood event; (**c**) The simulated accumulated precipitation (mm) as resulted from the WRF-ARW model, indicatively for the 8 hours from November 24 (22:00 local time) to November 25 (06:00 local time). The model also estimated the 1-hour precipitation amounts for the entire simulation period; (**d**) The RS results of the flood extent of the studied event of November 2019, according to the index RSWIR2.

The flood extent map that resulted from the RS analysis (Figure 4d) occurred by comparing all the computed Water Indices (WIs) and interpreting them with expert knowledge, while visually inspecting them alongside the 4 (Red)-3 (Green)-2 (Blue) natural composite of the corresponding S2 image, as mentioned in the Methodology section. The analysis showed that the Red and Short-Wave Infrared 2 Index (RSWIR2), with a threshold value of ≥ -0.1, was the most effective in detecting inundated areas, consistently producing stable results throughout the analysis.

The 2D HEC-RAS flood model ran for the flood of November 2019, according to the description provided in the previous section, combining the DEM and the area's topography, the *n* values, and the spatially distributed rainfall representing the simulated storm. The resulting flood inundation map of the hydraulic model (Figure 5) was compared with the RS flood extent result (as shown in Figure 4d). The validation of the HEC-RAS' results was assessed by the CSI scores (Equation (3)), which was 0.65. This indicates a satisfactory model performance, as *CSI* values above 0.5 are acceptable. The total simulated flood inundation area was 595,246 m^2, covering 24% of the total Kineta's town residential area, which is a significant portion of a small coastal town.

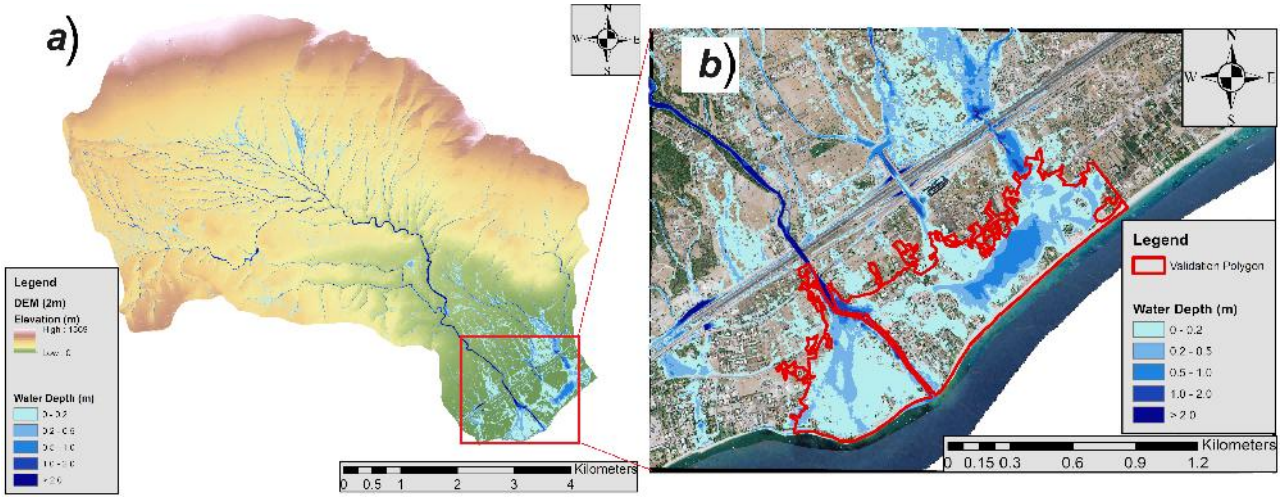

Figure 5. The hydraulic simulation results**.** (**a**) The extent of the flood in Kineta catchment; (**b**) The water extent and depth in the Kineta town. The red "validation polygon" represents the boundary of the water extent as resulted from RS analysis (shown in Figure 4d).

The proper installation of the appropriate PFPs for the area could have been the solution to mitigate this flood. In order to identify the most appropriate, we were based on the categorization of PFPs into land, channel and road and trail treatments (as mentioned in the methodology section). The PFP types under each category were assessed and further specified for the Kineta catchment, taking also into account the available Greek guidelines, and recent practical experiences from similar Mediterranean (and Greek) case studies [80–82]. Thus, the most appropriate PFPs were proposed. In particular:

- First, the road and trail treatments are targeting certain routes of high importance and can be expensive interventions. There are very few applications in Greece, following severe flood events, so in this case they were not considered. The most commonly applied PFPs in Greece are land treatments (especially barrier-based and channel-based), due to their relatively low costs, and ease of installation from local timber.
- Barrier-based methods: Among the different land treatments, most cover-based approaches (e.g., mulch, seeding, etc.) have not been used in Greece. In contrast, barrier-based methods are a common approach, involving the on-site installment of barriers to trap sediments, reduce excess flow, and slow runoff. The most common, easy-to-apply, and (reported to be) low-cost measures are the log-erosion barriers (LEBs). LEBs are suitable for areas with high-moderate burn severity, and slopes between 20%–50%. Often many applications consider the slope installation starting from 10%, with looser spacing till 20%, depending on the morphology of the site. They are usually 0.2 m high, and placed every about 8 m, continuously along the contour lines.

- Channel treatments: As mentioned, these are used mainly to protect critical downstream areas from floodwaters and sediments [83,84], so in our case where the downstream coastal area is the Kineta town, a residential area, this type of PFP is necessary. The most commonly applied channel treatments are wooden check-dams (smaller structures in more narrow streams), and concrete check-dams (larger structures in the main channels). The wooden check-dams are usually constructed along the channels of first- and second-order streams, namely the small tributaries, because they are more controllable in smaller channel openings, exhibit higher durability, and are more easily accessible, allowing thus their maintenance. Their typical height is 1 m, and they are placed in constrictions of channels having an upstream widened bed and a slight stream slope (<20%), spaced at intervals of 50–100 m, although this number is highly variable, depending on each area's morphology. The concrete check-dams are usually 2 to 2.5 m tall, and are typically built in the main channels to serve as a third-level protection measure. Due to the increased costs of the concrete check-dams, they are usually omitted.

For the studied case of Kineta catchment, LEBs and wooden check-dams were deemed to be the most appropriate, feasible and realistic, considering the area's characteristics, and according to the respective official Greek guidelines. Specifically, the Hellenic Technical Specification on the Technical Guidelines for erosion control structures, and relevant studies and technical reports describing the application of these PFPs [80–82], outline the main criteria for their installation. These refer to the burn severity categories (as described in the bullets above per case, and in our case estimated as in Figure 4), the stream slopes and order (as described in the bullets above per case, and in our case estimated as in Figure 6a, based on the DEM), while the spacing and final installation decisions are always according to the judgement of the on-field experts. Considering these, for the Kineta catchment, the LEBs were installed every 10 m, along the contour lines according to the usual practice followed in Greece. In particular, the evolution of the flood depth, and extent created during the hydraulic simulation allowed us to identify the streams that delivered significant floodwaters, which were mainly in the northeast part of the catchment. The water velocity was another factor that confirmed the need for more 'dense' protection of some streams, namely the ones in the northeast. To achieve this, we placed the wooden check-dams in the third-order streams, and also, in a continuous line with the LEBs, within the channels, throughout the whole catchment. So, overall, the wooden check-dams were installed within the small tributaries, i.e., the first-, second- and third-order streams, approximately every 10 m. This is a more conservative approach than usual (only in the first- and second-order streams, per 50–100 m), because the Kineta catchment is a small site, and its third-order streams are quite narrow. At the spots where the LEBs meet a stream, the installation of a wooden check-dam within these streams is applied, as mentioned, to form a continuous line of protection. Moreover, the knowledge of the flood inundation, as resulted from the hydraulic models (Figure 5), indicates that a significant amount of floodwater came from the northeast part of the catchment. The small streams contributing to the two channels that delivered the majority of the floodwater are suitable for the installation of wooden check-dams, so considering them in the third-order streams, approximately every 10 m, is expected to provide enhanced protection downstream, "blocking" a considerable amount of runoff. The spatial distribution of the PFPs designed is shown in Figure 6b.

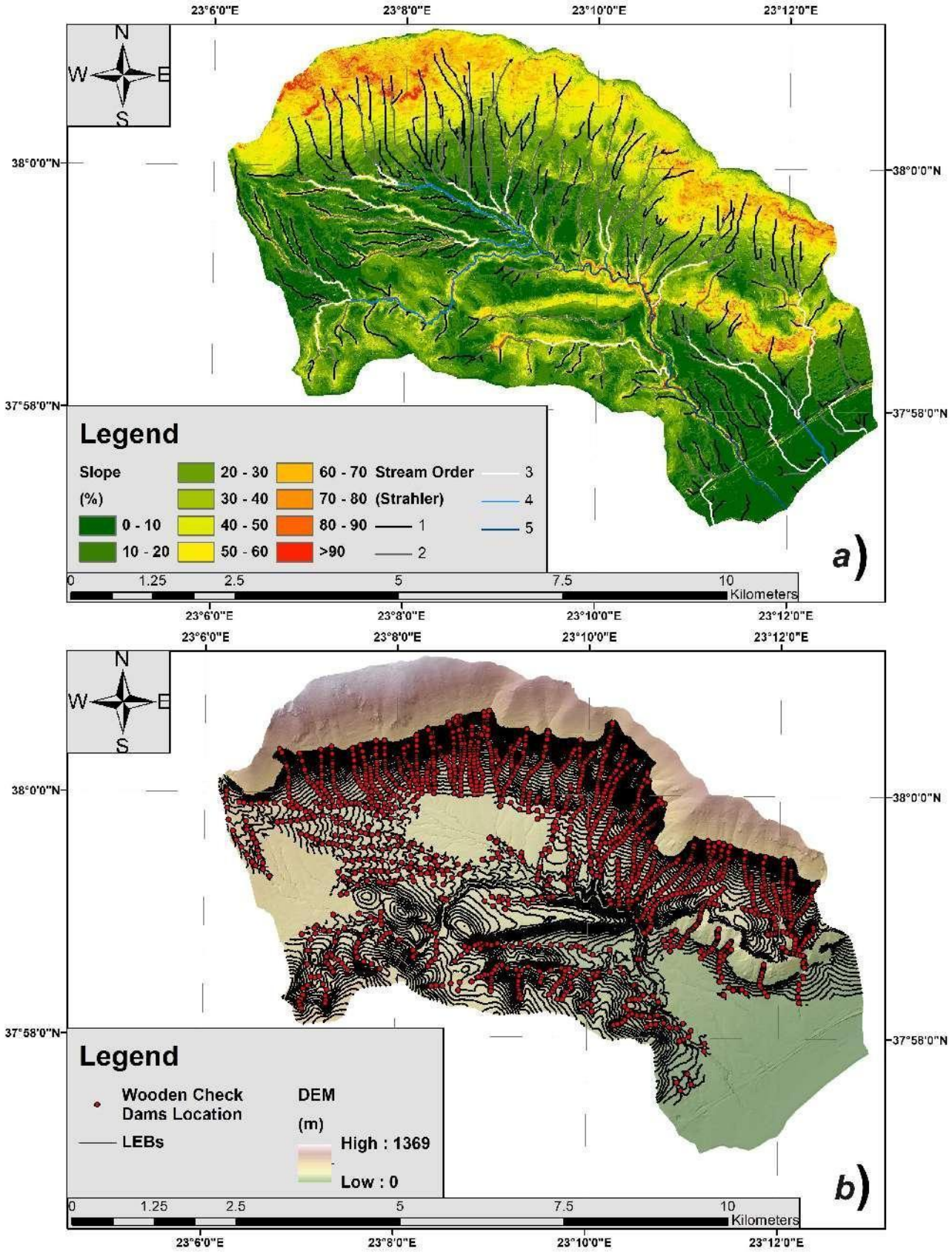

Figure 6. Designing the proposed works. (**a**) The stream order and slope were calculated based on the area's DEM within GIS, and together with the burn severity areas (as shown in Figure 4), to guide us in designing the PFPs; (**b**) The final map with the locations of the designed LEBs and wooden check-dams.

The total costs for the application of the designed PFPs (Figure 6b) took into account the necessary material and transportation costs, as well as the installation and labor costs. Following the recent destructive wildfires at large areas in Thrace, Northern Greece during the summer of 2023 [85,86], the Greek Ministry of Environment and Energy has issued a detailed set of studies reporting the on-site installation of post-fire restoration works in forests, including the associated costs [87]. The same approach is followed in this paper to estimate the cost for the implementation of the suggested PFPs (LEBs and wooden check-dams). The cost analysis reported (based on the joint Ministerial Decisions of the Greek Ministries of Infrastructure and Transport, and Environment and Energy, on the application of Forestry works), takes into account the costs of logging (i.e., timber), their transportation, and installation (construction), both for LEBs and wooden check-dams (as presented in Table 2). The values refer to €2023 and the use of pine trees is considered as timber, which is also common in the Kineta mountainous area.

Table 2. Cost analysis for LEBs and wooden check-dams, considering costs of materials (timber), transportation, and installation (construction), in values of 2023 [87].

Logging Costs (for pine-trees 2 m long × 0.2m diameter)
Timber cost: 7.99€
Increase 10% for burnt sites: 0.80€
Increase 10% due to execution by the same work group: 0.80€
Allowance 5% for travel expenses for a distance of 0–50 km: 0.40€
Good performance bonus 5%: 0.40€
Employer's insurance 24.44%: 2.54€

Logging cost: 12.93€/m^3
Displacement and transport costs (for pine-trees 2 m long × 0.2 m diameter)
Transport cost for distances less than 200 m: 8.98€
Increase 10% for burnt sites: 0.90€
Increase 10% due to execution by the same work group: 0.90€
Allowance 5% for travel expenses for a distance of 0–50 km: 0.44€
Good performance bonus 5%: 0.45€
Employer's insurance 24.44%: 2.85€

Transport costs: 14.53€/m^3
Estimation of LEBs construction cost per meter installed
Volume of a unit log (1 m long × 0.2 m diameter): 0.0314
Increase 10% for loss coverage and supporting brackets: 0.0345
Volume per meter installed: 0.066 m^3/m
Logging cost = 12.93€/m^3 · 0.066 m^3/m = 0.85€/m
Transport cost = 14.53€/m^3 · 0.066 m^3/m = 0.96€/m
Labour cost of an unskilled worker for digging, construction and installation 3.06€/m
----
Total cost per meter of LEBs installed: 4.87€/m
Estimation of wooden check-dam cost per square meter installed
The volume of timber required for a typical trapezoid wooden check-dam, using unit logs of typical dimensions as above, and supporting brackets and a log, tied with wires is estimated to be 1.635 m^3.
Logging cost = 12.93€/m^3 · 1.635m^3 = 21.14€/wooden check-dam
Transport cost = 14.53€/m^3 · 1.635m^3 = 23.76€/wooden check-dam
Labour cost of an unskilled worker and a logger for tools, digging, construction and installation 172.38€/m
----
Total cost of a wooden checked-dam of open surface of 3.5 m^2 = 172.38/3.5 = 49.25€/m^2

Based on these estimations, the costs for the PFPs designed (955,336 m of LEBs installed and 2035 wooden check-dams of 3.5 m^2 each — Figure 6b) for the Kineta catchment would be 4,652,486€ for the LEBs, plus 350,783€ for the wooden check-dams. This results in a total cost of 5,003,269€.

5. Conclusions

In this paper, a novel, integrated, and multidisciplinary framework was introduced for accurately assessing post-fire floods, simulating the fire's effect, and representing the flood event. Moreover, different PFPs were assessed, and the most appropriate were selected for the study area considering the available guidelines and the specific characteristics of the site and its response to the simulated flood. The presented framework mobilizes different approaches and uses new modeling tools, combining them for the first time, enhancing the accuracy of their application. The approach is easily transferable to other study areas worldwide, offering thus an improved understanding of the impacts of combined fire-flood disasters and relevant protection measures. Sediment transport is also another relevant factor, which is included in our future research plans, in order to provide more holistic assessments of these combined flood-sediment hazards, as well as the respective protection measures.

The PFPs designed in this study were developed as a flood mitigation strategy for the Kineta catchment, retrospectively, to propose a way to mitigate the effects of the flood of November 2019. Of course, the follow-up question of this research would be on the effectiveness of the PFPs: If these PFPs had been in place after the wildfire (in other words, if this investment of approximately 5 million euros had been done) would the flood have been avoided? Currently, we cannot really know. But in this paper, we showed for the first time that the protection can be designed based on comprehensive models, in a science-supported manner, and that it is possible with relatively low-cost measures. In order to answer such a question, this would require modeling the effectiveness of these PFPs to the flooding, as well as re-assessing the same flood under these hypothetical conditions (assuming the PFPs were in place). Modeling the PFPTs' effectiveness is a quite time- and computationally-demanding task, particularly challenging in incorporating the LEBs and the wooden check-dams in the terrain conditions of the hydraulic model. This is beyond the scope of this paper; however, it is considered in our future research plans. The answer to this question, whether the flood would have been avoided if these PFPs had been applied, is probably 'not entirely': Even if the PFPs were in place, the flood would not have been totally avoided. But it would have been mitigated, and hence we believe that the investment in flood protection is a worthy strategy to mitigate the flood risks.

Research has shown that stakeholders and communities are keen on adopting PFP measures but the lack of knowledge about their design or implementation creates hesitation [88]. So, we are optimistic that this study can serve as a starting point towards the timely consideration of PFPs, in an integrated and scientifically-supported way.

Author Contributions

Conceptualization, A.A. and G.P.; methodology and formal analysis, A.A., G.P., G.V., V.M. and A.P.; writing—original draft preparation, A.A., G.P., G.V., V.M. and A.P.; writing—review and editing, A.A., G.P., G.V., V.M., P.K., A.P., A.P. and E.D. All authors have read and agreed to the published version of the manuscript.

Funding

This work received no external funding.

Institutional Review Board Statement

Not applicable.

Informed Consent Statement

Not applicable.

Data Availability Statement

All data can be made available from the corresponding author upon request.

Conflicts of Interest

The authors declare no conflict of interest.

References

1. Goss, M.; Swain, D.L.; Abatzoglou, J.T.; Sarhadi, A.; Kolden, C.A.; Williams, A.P.; Diffenbaugh, N.S. Climate Change is Increasing the Likelihood of Extreme Autumn Wildfire Conditions across California. *Environ. Res. Lett.* **2020**, *15*, 094016. [CrossRef]
2. Alamanos, A.; Koundouri, P. Emerging Challenges and the Future of Water Resources Management. *Hydrolink, Citiz. Sci.*, *4*.
3. Alamanos, A. Megadroughts and Challenges for Water Resources Management. In *Elgar Encyclopedia of Water Policy, Economics and Management*; Koundouri, P., Alamanos, A., Eds.; Edward Elgar Publishing: Cheltenham, UK, 2024; pp. 164–167. [CrossRef]
4. Tuel, A., Eltahir, E.A. Why is the Mediterranean a Climate Change Hot Spot? *J. Clim.* **2020**, *33*, 5829–5843. [CrossRef]
5. Papagiannaki, K.; Giannaros, T.M.; Lykoudis, S.; Kotroni, V.; Lagouvardos, K. Weather-Related Thresholds for Wildfire Danger in a Mediterranean Region: The Case of Greece. *Agric. For. Meteorol.* **2020**, *291*, 108076. [CrossRef]
6. Ruffault, J.; Curt, T.; Moron, V.; Trigo, R.M.; Mouillot, F.; Koutsias, N.; Pimont, F.; Martin-StPaul, N.; Barbero, R.; Dupuy, J.L.; et al. Increased Likelihood of Heat-Induced Large Wildfires in the Mediterranean Basin. *Sci. Rep.* **2020**, *10*, 13790. [CrossRef]
7. Varela, V.; Vlachogiannis, D.; Sfetsos, A.; Karozis, S.; Politi, N.; Giroud, F. Projection of Forest Fire Danger Due to Climate Change in the French Mediterranean Region. *Sustainability* **2019**, *11*, 4284. [CrossRef]
8. Thomas, M.A.; Rengers, F.K.; Kean, J.W.; McGuire, L.A.; Staley, D.M.; Barnhart, K.R.; Ebel, B.A. Postwildfire Soil-Hydraulic Recovery and the Persistence of Debris Flow Hazards. *J. Geophys. Res.: Earth Surf.* **2021**, *126*. [CrossRef]
9. Nasirzadehdizaji, R.; Akyuz, D.E. Predicting the Potential Impact of Forest Fires on Runoff and Sediment Loads Using a Distributed Hydrological Modeling Approach. *Ecol. Modell.* **2022**, *468*, 109959, [CrossRef]
10. Santi, P.M.; deWolfe, V.G.; Higgins, J.D.; Cannon, S.H.; Gartner, J.E. Sources of Debris Flow Material in Burned Areas. *Geomorphology* **2008**, *96*, 310–321. [CrossRef]
11. Skilodimou, H.D.; Bathrellos, G.D.; Alexakis, D.E. Flood Hazard Assessment Mapping in Burned and Urban Areas. *Sustainability* **2021**, *13*, 4455. [CrossRef]
12. Zscheischler, J.; Westra, S.; van den Hurk, B.J.J.M.; Seneviratne, S.I.; Ward, P.J.; Pitman, A.; AghaKouchak, A.; Bresch, D.N.; Leonard, M.; Wahl, T.; et al. Future Climate Risk from Compound Events. *Nat. Clim. Change* **2018**, *8*, 469–477. [CrossRef]
13. Cramer, W.; Guiot, J.; Fader, M.; Garrabou, J.; Gattuso, J.P.; Iglesias, A.; Lange, M.A.; Lionello, P.; Llasat, M.C.; Paz, S.; et al. Climate Change and Interconnected Risks to Sustainable Development in the Mediterranean. *Nat. Clim. Change* **2018**, *8*, 972–980. [CrossRef]
14. Evelpidou, N.; Cartalis, C.; Karkani, A.; Saitis, G.; Philippopoulos, K.; Spyrou, E. A GIS-Based Assessment of Flood Hazard through Track Records over the 1886–2022 Period in Greece. *Climate* **2023**, *11*, 226. [CrossRef]
15. Alamanos, A.; Loukas, A.; Mylopoulos, N.; Xenarios, S.; Vasiliades, L.; Latinopoulos, D. Climate Change Effects on Agriculture in Southeast Mediterranean: The Case of Karla Watershed in Central Greece. *Geophys. Res. Abstr.* **2019**, *21*, 1.
16. Papaioannou, G.; Alamanos, A.; Maris, F. Evaluating Post-Fire Erosion and Flood Protection Techniques: A Narrative Review of Applications. *GeoHazards* **2023**, *4*, 380–405. [CrossRef]
17. Brogan, D.J.; Nelson, P.A.; MacDonald, L.H. Spatial and Temporal Patterns of Sediment Storage and Erosion Following a Wildfire and Extreme Flood. *Earth Surf. Dyn.* **2019**, *7*, 563–590. [CrossRef]
18. Kinoshita, A.M.; Hogue, T.S.; Napper, C. Evaluating Pre- and Post-Fire Peak Discharge Predictions across Western U.S. Watersheds. *J. Am. Water Resour. Assoc.* **2014**, *50*, 1540–1557. [CrossRef]
19. Shen, X.; Anagnostou, E.N.; Allen, G.H.; Robert Brakenridge, G.; Kettner, A.J. Near-Real-Time Non-Obstructed Flood Inundation Mapping Using Synthetic Aperture Radar. *Remote Sens. Environ.* **2019**, *221*, 302–315. [CrossRef]
20. Ghimire, G.R.; Jadidoleslam, N.; Goska, R.; Krajewski, W.F. Insights into Storm Direction Effect on Flood Response. *J. Hydrol.* **2021**, *600*, 126683. [CrossRef]
21. Hou, J.; Guo, K.; Liu, F.; Han, H.; Liang, Q.; Tong, Y.; Li, P. Assessing Slope Forest Effect on Flood Process Caused by a Short-Duration Storm in a Small Catchment. *Water* **2018**, *10*, 1256. [CrossRef]
22. Skamarock, C.; Klemp, B.; Dudhia, J.; Gill, O.; Liu, Z.; Berner, J.; Wang, W.; Powers, G.; Duda, G.; Barker, D.; et al. *A Description of the Advanced Research WRF Model Version 4.3*; NCAR Tech Note, NCAR/TN–556+ STR; National Center for Atmospheric Research: Boulder, CO, USA, 2021. [CrossRef]

23. Singh, K.S.; Albert, J.; Bhaskaran, P.K.; Alam, P. Assessment of Extremely Severe Cyclonic Storms over Bay of Bengal and Performance Evaluation of ARW Model in the Prediction of Track and Intensity. *Theor. Appl. Climatol.* **2021**, *143*, 1181–1194. [CrossRef]
24. Douluri, D.L.; Chakraborty, A. Assessment of WRF-ARW Model Parameterization Schemes for Extreme Heavy Precipitation Events Associated with Atmospheric Rivers over West Coast of India. *Atmos. Res.* **2021**, *249*, 105330. [CrossRef]
25. Varlas, G.; Papadopoulos, A.; Papaioannou, G.; Markogianni, V.; Alamanos, A.; Dimitriou, E. Integrating Ensemble Weather Predictions in a Hydrologic-Hydraulic Modelling System for Fine-Resolution Flood Forecasting: The Case of Skala Bridge at Evrotas River, Greece. *Atmosphere* **2024**, *15*, 120. [CrossRef]
26. Tewari, M.; Boulder, C.; Chen, F.; Wang, W.; Dudhia, J.; LeMone, M.; Mitchell, K.; Ek, M.; Gayno, G.; Wegiel, J.; et al. Implementation and Verification of the Unified Noah Land Surface Model in the WRF Model. In Proceedings of the 20th Conference on Weather Analysis and Forecasting/16th Conference on Numerical Weather Prediction, Seattle, WA, USA, 12–16 January 2004; pp. 11–15.
27. Kabenge, M.; Elaru, J.; Wang, H.; Li, F. Characterizing Flood Hazard Risk in Data-Scarce Areas, Using a Remote Sensing and GIS-Based Flood Hazard Index. *Nat. Hazards* **2017**, *89*, 1369–1387. [CrossRef]
28. Alamanos, A.; Linnane, S. Drought Monitoring, Precipitation Statistics, and Water Balance with Freely Available Remote Sensing Data: Examples, Advances, and Limitations. In Proceedings of the Irish National Hydrology Conference 2021, Athlone, Ireland, 2021; pp. 1–13.
29. Moreno, H.A.; Gourley, J.J.; Pham, T.G.; Spade, D.M. Utility of Satellite-Derived Burn Severity to Study Short- and Long-Term Effects of Wildfire on Streamflow at the Basin Scale. *J. Hydrol.* **2020**, *580*, 124244. [CrossRef]
30. Kurbanov, E.; Vorobev, O.; Lezhnin, S.; Sha, J.; Wang, J.; Li, X.; Cole, J.; Dergunov, D.; Wang, Y. Remote Sensing of Forest Burnt Area, Burn Severity, and Post-Fire Recovery: A Review. *Remote Sens.* **2022**, *14*, 4714. [CrossRef]
31. Chuvieco, E.; Aguado, I.; Salas, J.; García, M.; Yebra, M.; Oliva, P. Satellite Remote Sensing Contributions to Wildland Fire Science and Management. *Curr. For. Rep.* **2020**, *6*, 81–96. [CrossRef]
32. Chawan, A.C.; Kakade, V.K.; Jadhav, J.K. Automatic Detection of Flood Using Remote Sensing Images. *J. Inf. Technol. Digital World* **2020**, *2*, 11–26.
33. Hashemi-Beni, L.; Gebrehiwot, A.A. Flood Extent Mapping: An Integrated Method Using Deep Learning and Region Growing Using UAV Optical Data. *IEEE J. Sel. Top. Appl. Earth Obs. Remote Sens.* **2021**, *14*, 2127–2135. [CrossRef]
34. Hamidi, E.; Peter, B.G.; Muñoz, D.F.; Moftakhari, H.; Moradkhani, H. Fast Flood Extent Monitoring With SAR Change Detection Using Google Earth Engine. *IEEE Trans. Geosci. Remote Sens.* **2023**, *61*, 1–19. [CrossRef]
35. Milišić, H.; Hadžić, E.; Šuvalija, S.; Jahić, E. Floodplain Mapping Using HEC-RAS and Lidar Data: A Case Study of Bistrica River (Vrbas River Basin in B&H). In Proceedings of the New Technologies, Development and Application IV, Sarajevo, Bosnia and Herzegovina, 24–26 June 2021; pp. 1093–1103. [CrossRef]
36. Papaioannou, G.; Vasiliades, L.; Loukas, A.; Alamanos, A.; Efstratiadis, A.; Koukouvinos, A.; Tsoukalas, I.; Kossieris, P. A Flood Inundation Modeling Approach for Urban and Rural Areas in Lake and Large-Scale River Basins. *Water* **2021**, *13*, 1264. [CrossRef]
37. Costabile, P.; Costanzo, C.; Ferraro, D.; Macchione, F.; Petaccia, G. Performances of the New HEC-RAS Version 5 for 2-D Hydrodynamic-Based Rainfall-Runoff Simulations at Basin Scale: Comparison with a State-of-the Art Model. *Water* **2020**, 12, 2326. [CrossRef]
38. Alamanos, A. Exploring the Impact of Future Land Uses on Flood Risks and Ecosystem Services, with Limited Data: Coupling a Cellular Automata Markov (CAM) Model, with Hydraulic and Spatial Valuation Models. *Qeios* **2024**. [CrossRef]
39. Yalcin, E. Assessing the Impact of Topography and Land Cover Data Resolutions on Two-Dimensional HEC-RAS Hydrodynamic Model Simulations for Urban Flood Hazard Analysis. *Nat. Hazards* **2020**, *101*, 995–1017. [CrossRef]
40. Earle, H.; Gunster, S. Fire and Climate: Connecting the Dots in British Columbia News Media. *Can. J. Commun.* **2021**, *46*, 961–982. [CrossRef]
41. Ebel, B.A.; Shephard, Z.M.; Walvoord, M.A.; Murphy, S.F.; Partridge, T.F.; Perkins, K.S. Modeling Post-Wildfire Hydrologic Response: Review and Future Directions for Applications of Physically Based Distributed Simulation. *Earth's Future* **2023**, *11*, e2022EF003038. [CrossRef]
42. Ebel, B.A. The Statistical Power of Post-Fire Soil-Hydraulic Property Studies: Are We Collecting Sufficient Infiltration Measurements after Wildland Fires? *J. Hydrol.* **2022**, *612*, 128019. [CrossRef]
43. Kastridis, A.; Stathis, D. Evaluation of Hydrological and Hydraulic Models Applied in Typical Mediterranean Ungauged Watersheds Using Post-Flash-Flood Measurements. *Hydrology* **2020**, *7*, 12. [CrossRef]
44. Lopes, A.R.; Girona-García, A.; Corticeiro, S.; Martins, R.; Keizer, J.J.; Vieira, D.C.S. What Is Wrong with Post-Fire Soil Erosion Modelling? A Meta-Analysis on Current Approaches, Research Gaps, and Future Directions. *Earth Surf. Processes Landforms* **2021**, *46*, 205–219. [CrossRef]

45. De Girolamo, A.M.; Cerdan, O.; Grangeon, T.; Ricci, G.F.; Vandromme, R.; Porto, A.L. Modelling Effects of Forest Fire and Post-Fire Management in a Catchment Prone to Erosion: Impacts on Sediment Yield. *Catena* **2022**, *212*, 106080. [CrossRef]
46. Rulli, M.C.; Offeddu, L.; Santini, M. Modeling Post-Fire Water Erosion Mitigation Strategies. *Hydrol. Earth Syst. Sci.* **2013**, *17*, 2323–2337. [CrossRef]
47. Prats, S.A.; Malvar, M.C.; Wagenbrenner, J.W. Compaction and Cover Effects on Runoff and Erosion in Post-Fire Salvage Logged Areas in the Valley Fire, California. *Hydrol. Processes* **2021**, *35*, e13997. [CrossRef]
48. Margiorou, S.; Kastridis, A.; Sapountzis, M. Pre/Post-Fire Soil Erosion and Evaluation of Check-Dams Effectiveness in Mediterranean Suburban Catchments Based on Field Measurements and Modeling. *Land* **2022**, *11*, 1705. [CrossRef]
49. Kastridis, A.; Kamperidou, V. Evaluation of the Post-Fire Erosion and Flood Control Works in the Area of Cassandra (Chalkidiki, North Greece). *J. For. Res.* **2015**, *26*, 209–217. [CrossRef]
50. O'Connell, P.E.; O'Donnell, G. Towards Modelling Flood Protection Investment as a Coupled Human and Natural System. *Hydrol. Earth Syst. Sci.* **2014**, *18*, 155–171. [CrossRef]
51. Koundouri, P. The Case for Declining Long-Term Discount Rates in the Evaluation of Flood-Defence Investments. In *Coping with Water Deficiency: From Research to Policymaking With Examples from Southern Europe, the Mediterranean and Developing Countries*; Koundouri, P., Ed.; Springer: Dordrecht, Netherlands, 2008; pp. 157–163. [CrossRef]
52. Kastridis, A.; Margiorou, S.; Sapountzis, M. Check-Dams and Silt Fences: Cost-Effective Methods to Monitor Soil Erosion under Various Disturbances in Forest Ecosystems. *Land* **2022**, *11*, 2129. [CrossRef]
53. Warziniack, T.; Thompson, M. Wildfire Risk and Optimal Investments in Watershed Protection. *West. Econ. Forum* **2013**, *12*, 19–28. [CrossRef]
54. Kineta Climate: Average Temperature by Month, Kineta Water Temperature. Available online: https://en.climate-data.org/europe/greece/kineta/kineta-281130/ (accessed on 10 July 2024).
55. Lekkas, E.; Spyrou, N.; Filis, C.; Diakakis, M.; Vassilakis, E.; Katsetsiadou, A.; Milios, D.; Arianoutsou, M.; Faragitakis, G.; Christopoulou, A.; et al. *The November 25, 2019 Kineta (Western Attica) Flood*; Athens, Greece, 2019; (In Greek).
56. Vimaonline Kineta is a barren land after the fire—The fire was rekindled. Vimaonline (In Greek). Available online: https://www.vimaonline.gr/20/article/33316/kraniou-topos-i-kineta-apo-tin-purkagia-anazopurothike-i-fotia (accessed on 8 November 2023).
57. Protothema Storm "Girionis": How Kineta was burned—Visual inspection in the area. ProtoThema 2019 (In Greek). Available online: https://www.protothema.gr/webtv/default-folder/3715449/kakokairia-giryonis-pws-i-pyrkagia-epnikse-tin-kineta/ (accessed on 8 November 2023).
58. Eleftheros typos The fire in Kineta started from the electricity piles—Details of the report. Eleftheros Typos 2019 (In Greek). Available online: https://www.panhellenicpost.com/2018/09/14/%CE%B1%CF%80%CF%8C-%CE%BA%CE%B1%CE%BB%CF%8E%CE%B4%CE%B9%CE%B1-%CF%84%CE%B7%CF%82-%CE%B4%CE%B5%CE%B7-%CE%B7-%CF%86%CF%89%CF%84%CE%B9%CE%AC-%CF%83%CF%84%CE%B7%CE%BD-%CE%BA%CE%B9%CE%BD%CE%AD%CF%84%CE%B1/ (accessed on 8 November 2023).
59. Alamanos, A.; Papaioannou, G.; Varlas, G.; Markogianni, V.; Papadopoulos, A.; Dimitriou, E. Representation of a Post-Fire Flash-Flood Event Combining Meteorological Simulations, Remote Sensing, and Hydraulic Modeling. *Land* **2024**, *13*, 47. [CrossRef]
60. Hui, P.; Li, Y.; Chen, Y.; Zhang, L.; Wei, F.; Wang, S.; Tang, J. The Impact of Radiation Parameterization Schemes on the Regional Climate Simulations over the CORDEX-EA Domain. *Atmos. Res.* **2019**, *224*, 81–98. [CrossRef]
61. Lekhadiya, H.S.; Jana, R.K. Analysis of Extreme Rainfall Event with Different Microphysics and Parameterization Schemes in WRF Model. *Positioning* **2018**, *9*, 1. [CrossRef]
62. Grell, G.A.; Freitas, S.R. A Scale and Aerosol Aware Stochastic Convective Parameterization for Weather and Air Quality Modeling. *Atmos. Chem. Phys.* **2014**, *14*, 5233–5250. [CrossRef]
63. Hong, S.Y.; Noh, Y.; Dudhia, J. A New Vertical Diffusion Package with an Explicit Treatment of Entrainment Processes. *Mon. Weather Rev.* **2006**, *134*, 2318–2341. [CrossRef]
64. Copernicus The Sentinels Scientific Data Hub. Available online: https://scihub.copernicus.eu/maintenance.html#/home (accessed on 2 February 2023).
65. Cui, L.; Li, G.; Ren, H.; He, L.; Liao, H.; Ouyang, N.; Zhang, Y. Assessment of Atmospheric Correction Methods for Historical Landsat TM Images in the Coastal Zone: A Case Study in Jiangsu, China. *Eur. J. Remote Sens.* **2014**, *47*, 701–716. [CrossRef]
66. Alcaras, E.; Costantino, D.; Guastaferro, F.; Parente, C.; Pepe, M. Normalized Burn Ratio Plus (NBR+): A New Index for Sentinel-2 Imagery. *Remote Sens.* **2022**, *14*, 1727. [CrossRef]

67. Amos, C.; Ferentinos, K.P.; Petropoulos, G.P.; Srivastava, P.K. Assessing the Use of Sentinel-2 in Burnt Area Cartography. In *Techniques for Disaster Risk Management and Mitigation*, 1st ed.; Srivastava, P.K., Singh, S.K., Mohanty, U.C., Murty, T.; John Wiley & Sons: Hoboken, NJ, USA, 2020; pp. 141–150. [CrossRef]
68. Rahman, S.; Chang, H.C.; Hehir, W.; Magilli, C.; Tomkins, K. Inter-Comparison of Fire Severity Indices from Moderate (Modis) and Moderate-to-High Spatial Resolution (Landsat 8 & Sentinel-2A) Satellite Sensors. In Proceedings of the 2018 IEEE International Geoscience and Remote Sensing Symposium, Valencia, Spain, 22–27 July 2018; pp. 2873–2876. [CrossRef]
69. Pekel, J.F.; Cottam, A.; Gorelick, N.; Belward, A.S. High-Resolution Mapping of Global Surface Water and Its Long-Term Changes. *Nature* **2016**, *540*, 418–422. [CrossRef]
70. Xu, H. Modification of Normalised Difference Water Index (NDWI) to Enhance Open Water Features in Remotely Sensed Imagery. *Int. J. Remote Sens.* **2006**, *27*, 3025–3033. [CrossRef]
71. National Cadastre and Mapping Agency, S.A. Organizations—GEODATA.Gov.Gr. Available online: https://Geodata.Gov.Gr/En/Organization/Ekxa (accessed on 4 March 2024).
72. Kalyanapu, A.; Burian, S.; McPherson, T. Effect of Land Use-Based Surface Roughness on Hydrologic Model Output. *J. Spat. Hydrol.* **2009**, 9, 51–71.
73. Canfield, H.E.; Goodrich, D. *Suggested Changes to AGWA to Account for Fire (V 2.1)*; USDA-ARS Southwest Watershed Research Center: Tucson, AZ, USA, 2005.
74. Sanz-Ramos, M.; Bladé, E.; González-Escalona, F.; Olivares, G.; Aragón-Hernández, J.L. Interpreting the Manning Roughness Coefficient in Overland Flow Simulations with Coupled Hydrological-Hydraulic Distributed Models. *Water* **2021**, *13*, 3433. [CrossRef]
75. Horritt, M.S.; Di Baldassarre, G.; Bates, P.D.; Brath, A. Comparing the Performance of a 2-D Finite Element and a 2-D Finite Volume Model of Floodplain Inundation Using Airborne SAR Imagery. *Hydrol. Processes* **2007**, *21*, 2745–2759. [CrossRef]
76. Costabile, P.; Costanzo, C.; Ferraro, D.; Barca, P. Is HEC-RAS 2D Accurate Enough for Storm-Event Hazard Assessment? Lessons Learnt from a Benchmarking Study Based on Rain-on-Grid Modelling. *J. Hydrol.* **2021**, *603*, 126962. [CrossRef]
77. Wagenbrenner, J.W.; Ebel, B.A.; Bladon, K.D.; Kinoshita, A.M. Post-Wildfire Hydrologic Recovery in Mediterranean Climates: A Systematic Review and Case Study to Identify Current Knowledge and Opportunities. *J. Hydrol.* **2021**, *602*, 126772. [CrossRef]
78. Napper, C. *Burned Area Emergency Response Treatments (BAER) Catalog*; US Forest Service: Washington, DC, USA; San Dimas Technology and Development Center: San Dimas, CA, USA, 2006.
79. Meteo Meteosearch | Weather Data Portal. Available online: https://meteosearch.meteo.gr/ (accessed on 13 April 2024).
80. Greek Ministry of Environment and Energy Hellenic Technical Specification on the Technical Guidelines for Temporary Erosion Control Structures Utilizing Locally Available Timber. ICS: 93.040; Athens Greece, 2009; 2009.
81. Papakonstantinou, S.; Kalliris, M. Flood and Soil-Erosion Protection Works in Forests Burned by the Wildfire of 27-07-2013 at the Communities of Istrio, Profilias, Arnithas, Vatiou, and Apolakkias, in Southern Rhodes. Decentralized Administration of the Aegean (in Greek); 2013.
82. Marougklianis, C.; Ranis, G. Final Study for the Construction of Wooden Check-Dams in the Forests of the Catchments of Rahonio, Prinou, Sotiros, and Kallirachis, Affected by the Wildfire of 10-09-2016 in Thasos Island. Decentralized Administration of Macedonia and Thrace (in Greek); 2018.
83. Myronidis, D.I.; Arabatzis, G. Evaluation of Greek Post-Fire Erosion Mitigation Policy through Spatial Analysis. *Pol. J. Environ. Stud.* **2009**, *18*, 865–872.
84. Myronidis, D.I.; Emmanouloudis, D.A.; Mitsopoulos, I.A.; Riggos, E.E. Soil Erosion Potential after Fire and Rehabilitation Treatments in Greece. *Environ. Model. Assess.* **2010**, *15*, 239–250. [CrossRef]
85. Koudoumakis, P.; Keramitsoglou, K.; Protopapas, A.L.; Dokas, I. A General Method for Multi–Hazard Intensity Assessment for Cultural Resources: Implementation in the Region of Eastern Macedonia and Thrace, Greece. *Int. J. Disaster Risk Reduct.* **2024**, *100*, 104197. [CrossRef]
86. Politi, N.; Vlachogiannis, D.; Sfetsos, A.; Gounaris, N.; Varela, V. Investigation of Fire Weather Danger under a Changing Climate at High Resolution in Greece. *Sustainability* **2023**, *15*, 2498. [CrossRef]
87. Greek Ministry of Environment and Energy Study on Soil-Erosion and Flood Protection Works at the Burnt Area of the Avantas Catchment and Surounding Settlements. Decentralized Administration of Macedonia and Thrace. (in Greek); 2023.
88. Karasmanaki, E.; Mallinis, G.; Mitsopoulos, I.; Karteris, A.; Chrysafis, I.; Bakaloudis, D.; Kokkoris, I.P.; Maris, F.; Arianoutsou, M.; Goldammer, J.G.; et al. Proposing a Governance Model for Environmental Crises. *Land* **2023**, *12*, 597. [CrossRef]